Diamond & Related Materials 127 (2022) 109144

Contents lists available at ScienceDirect

Diamond & Related Materials

journal homepage: www.elsevier.com/locate/diamond

Improving the reliability of power LEDs with diamond boards

Shusmitha Kyatam, Luis Rodrigues, Stanislav Maslovski, Luis N. Alves, Joana C. Mendes *

Instituto de Telecomunicações e Departamento de Electrónica, Telecomunicações e Informática, University of Aveiro, Aveiro 3810-193, Portugal

ARTICLE INFO

2000 MSC:
0000 1111

PACS:
72.15.Eb
81.05.ug
85.60.Jb
81.15.Gh

Keywords:
Diamond board
Power LED
Thermal management
Reliability

ABSTRACT

Despite being efficient devices, when compared to other light sources, high power light emitting diodes (LEDs) suffer from heating effects that have a negative impact on their reliability. Power LEDs are typically assembled on metal core printed circuit boards (MCPCBs) to facilitate the extraction of the heat. Diamond boards can also be used for the same purpose, since diamond is the best isotropic conductor of heat known to man and simultaneously an electrical insulator. In order to evaluate the impact of the boards on the device lifetime, high power Cree LEDs were mounted on FR4, MCPCB, and diamond boards. The case temperature was measured for different current ratings, and the aging acceleration factor of the devices mounted on FR4 and diamond boards was estimated relatively to the LEDs mounted on the MCPCB boards. Diamond boards were shown to have a tremendous impact on the lifetime; for the nominal current level, and depending on the activation energy of the aging processes, the LEDs mounted on diamond boards age 60–80 % slower than their counterparts mounted on the MCPCB boards.

1. Introduction

High power light emitting diodes (LEDs) have become the main light source in every day applications. These compact devices have a large lighting capability and spend only a fraction of the energy required to power filament bulbs, nevertheless self-heating is one of the most limiting issues of power LEDs. Although lighting LEDs do not emit IR radiation directly, at high levels of current, the non-radiative recombination processes and the parasitic ohmic losses in the contacts and cladding layers cannot be neglected and it is estimated that 75 % of the electric power is converted into heat [1]. The LED die is typically encapsulated inside a dome-shaped material with a large refractive index. This dome improves the extraction of light from the device; however, dome materials are also poor conductors of heat, which creates an additional issue since convection may no longer be used to remove the heat away from the junction. Both LED manufacturers and circuit designers have come up with a variety of creative strategies to carry the heat away of the junction and guarantee that the junction temperature T_J remains as low as possible during device operation.

At system level, the temperature may be controlled with a thermoelectric cooler. These devices can be used together with fans [2] or thermoelectric generators [3], allowing the thermal energy dissipated by the LED to be partially recycled. Heat sinks (HS) are another possibility; as examples, the impact of using graphene-coated [4] and honey comb HSs [5] has been evaluated numerically. A HS with integrated heat pipes has also been proposed and verified experimentally [6].

At circuit level the use of power boards should be taken into consideration. Ceramic boards [7] as well as metal core printed circuit boards (MCPCBs) are two of the options available to the circuit designer. They can be complemented with thermal microvias [8] or heat pipes [9]. Huang *et al.* [10] used polymer-filled composites to further enhance radiative heat transfer from the board. Different approaches have also been proposed to minimize the package thermal resistance. The efficiency of a power package was increased by 3 % by including a copper (Cu) heat spreader [11]. When attaching the LED die to the carrier, replacing wire bonding with flip chip improves the extraction of heat from the LED die, especially if combined with sub-mounts with large thermal conductivity (λ). Different sub-mount materials have been proposed, such as alumina (Al_2O_3) [12], silicon (Si) [13], aluminium nitride (AlN) [14,15], and diamond [16]. The LED die has been further integrated with a Si TEC MEMS using flip-chip [17] and the impact of the solder pads, solder bumps, die attach, and underfills [4,12,13,15,18] has also been evaluated.

Thanks to properties such as high bandgap (5.4 eV), breakdown electric field (2×10^7 V/cm), and λ (1800–2000 W/(m·K) [19]), diamond comes as a candidate to improve the thermal management of power devices. The use of diamond as a HS has been proposed in 1967; in comparison with regular Cu HSs, its use doubled the continuous

* Corresponding author.
E-mail address: joanacatarina.mendes@ua.pt (J.C. Mendes).

https://doi.org/10.1016/j.diamond.2022.109144
Received 23 February 2022; Received in revised form 12 May 2022; Accepted 28 May 2022
Available online 5 June 2022

power density of Si avalanche diodes [20]. Diamond has also been used to improve the thermal management of power LEDs at different levels. Horng *et al.* [11] mounted the LED die on an aluminium (Al) board coated with a diamond-like layer and obtained an 11 °C reduction in T_J at 350 mA in comparison to mounting the LED on a conventional MCPCB. Chen *et al.* [21] reported a 20 °C reduction in T_J at 1 A when the LED chips were bonded to Si substrates coated with 20 μm of diamond. Fan *et al.* [22] replaced the Cu HS of white power LEDs with a diamond/Cu composite material and the weight of the internal HS was reduced by more than 35 %; simultaneously the thermal resistance and T_J decreased 10.5 % and 33.3 %, respectively. Diamond films have also been integrated in grooves etched on the upper ITO layer of LEDs [23]. The replacement of the AlN carrier of Cree XLamp XB-D LEDs with a diamond plate is estimated to improve the lifetime of the devices by 25 % and 50 % for 350 (nominal current) and 800 mA, respectively, and to decrease the drift of the wavelength with the current level [16].

Despite the promising results of these different approaches, the use of diamond plates as a printed circuit boards (PCBs) to directly assemble surface mount components has not, to the authors' best knowledge, been reported yet. This manuscript aims at filling this gap. To this end, Cree cold white XLamp XB-D LEDs were mounted on common FR4, MCPCB, and diamond boards and the impact of the different boards on the T_J and lifetime of the devices was estimated. The manuscript is organized as follows: the LEDs and the experimental setup implemented to measure T_J are described in Section 2. An analytical model for the heat transport in the considered setup is presented in Section 3. The experimental results are presented and discussed in Section 4 and the conclusions of the work are summarized in Section 5.

2. Experimental

2.1. LED and boards layout

Cold white XLamp XB-D LEDs were purchased from Cree. These LEDs have a maximum current rating of 1 A and a small footprint (2.45 × 2.45 mm^2). The cross-section view of an individual LED is shown in Fig. 1a. The LED die (in blue color) is composed by a silicon carbide (SiC) substrate on which the gallium nitride (GaN) active layers were deposited [16]. The LED die is attached to an AlN carrier (in grey); the LED junction terminals and the electrodes deposited on the top surface of the carrier are electrically connected via wire bonds (red shapes). Electrical vias (not shown) connect electrically the electrodes on the carrier top surface to the external anode and cathode terminals at the back of the LED package and a thermal pad in the middle facilitates the removal of heat generated during the device operation.

Different 1 cm^2 boards were prepared according to the electrode layout suggested in the datasheet [24] (0.8 and 1.6 mm-thick FR4, MCPCB, and diamond) (Fig. 1a, Sch1); a set of FR4 boards with thermal pads was also prepared (Fig. 1a, Sch2). The material, thickness, and λ of each layer are listed in Table 1. The LEDs were mounted on FR4/MCPCB boards using lead-free solder (Fig. 1b). Initially they were mounted on the diamond board using the same solder, however a few trials were required to optimize the procedure and the top gold (Au) layer was eventually removed during the failed attempts. As a consequence, only titanium (Ti)/tungsten (W) layers with a track resistance higher than 200 Ω remained. Following this experimental issue, the tracks on the diamond board were covered with silver (Ag) conductive paint and the LEDs were mounted directly on that layer.

2.2. Temperature measurements

The boards were mounted on a HS with a Cu core and Al fins (Fig. 2a) (with a height/outer diameter of 2/3 and 2.5/8 cm, respectively) by means of CPU thermal paste (λ = 12.5 W/(mK)). Two FR4 flaps were attached to the HS to facilitate the mounting and removal of each board – marked by green arrows in Fig. 2a – and the temperature of the thermal pad (hereafter referred to as solder point temperature, T_{SP}) was measured by a type K thermocouple placed close to the LED case (red arrow in Fig. 2a), according to the instructions provided by the manufacturer [25]. The HS was attached to a metallic frame (Fig. 2b) and a second type K thermocouple attached to the frame (not shown) measured the ambient temperature during the experiments.

The evolution of T_{SP} and LED voltage as a response to different current steps was monitored by a custom-made electronic module composed of a PC, a driver and acquisition module, and the LED + PCB mounted on the HS. The PC asks for the desired system parameters (target LED current, step time) and receives/stores the measured data (LED current, voltage, and T_{SP}). All the control and acquisition tasks are performed by the driver and acquisition module, which comprises a microcontroller (Texas Instruments MSP430FR5994) embedded in a development board (Texas Instruments MSP-EXP430FR5994), a current driver, a differential voltage amplifier (INA2133UA), a current sensor (TMCS1100A4QDR), and a thermocouple amplifier (AD595), pre-calibrated for type K thermocouples. The three readings (current, voltage, and T_{SP}) are sequentially read by the microcontroller built-in ADC with time intervals of 0.1 s and sent to MatLab via serial port. The T_{SP} and voltage of LEDs mounted on different boards were measured as a response to current steps between 100 and 700 mA with a step of 100 mA and also for 350 mA (datasheet nominal current). The LEDs were allowed to cool down to room temperature between successive measurements.

3. Analytical thermal model

In this section, we will formulate an equivalent thermal model for the LED mounted on different substrates considered in the experimental studies outlined in the previous section. To develop such a model, a number of simplifying assumptions have to be made. First, we assume that the λ of the substrate materials such as metals and solid dielectrics can be considered constant with temperature. For metals such as Cu, this assumption is well justified because the variation of conductivity with temperature is low within the relatively narrow range of temperatures we are interested in. The same can be said about the ceramic and diamond substrates. Regarding the FR4 substrate — which is a composite material formed by fiberglass and epoxy resin — there is simply no reliable data on the variation of λ of this complex material with temperature. Also, it has to be mentioned that FR4 is not a specific substrate material: FR4 is just a NEMA[1] grade of material. The properties of particular FR4 grade materials depend on the epoxy content, glass weave thickness and type, and many other factors. Moreover, the λ of FR4 materials is anisotropic, with an in-plane component that is three to four times larger than the out-of-plane component. Therefore, in the FR4 board case we are limited to using an empirical value of the conductivity in the range from 0.2 to 1.0 W/(m·K).

In order to take into account cooling due to air convection, we assume that the models of heat convection used for the electronic components mounted on a PCB can be also used in our case [30]. In such models, the convection is taken into account by an equivalent heat transfer coefficient (natural convection heat transfer coefficient) that depends on the temperature gradient and the dimensions of the PCB with electronic components. For vertical plates and cylinders, the natural convection heat transfer coefficient can be expressed as

$$h_c = \xi \cdot \left(\frac{\Delta T}{L}\right)^{1/4}, \tag{1}$$

where $\xi = 1.42\ \mathrm{W} \cdot m^{-7/4} \cdot K^{-5/4}$ is an empirical constant [30], ΔT is the difference between the hot object temperature and the ambient air temperature, and L is the vertical dimension of the plate or the length of

[1] NEMA stands for National Electrical Manufacturers Association.

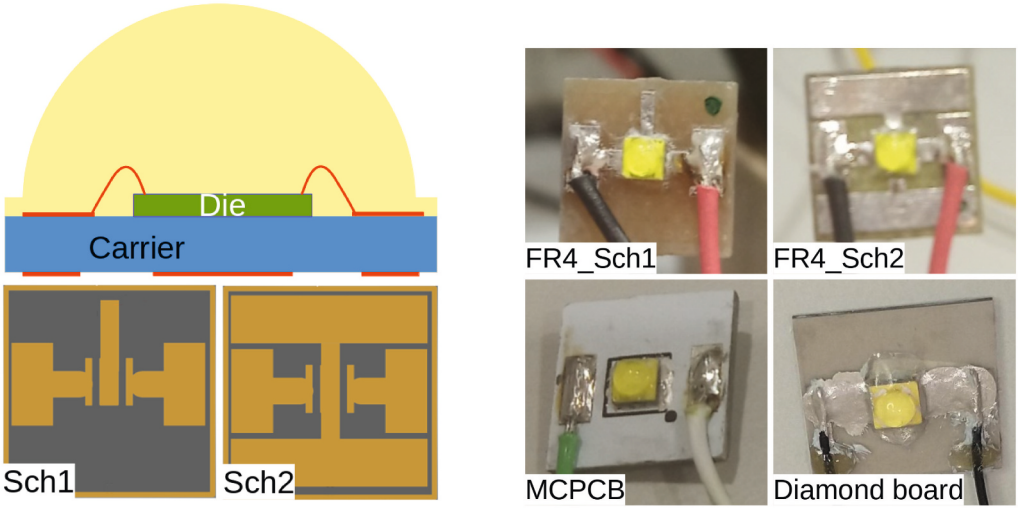

Fig. 1. (a, top) LED cross-section view (drawing not to scale). (a, bottom) Electrodes layout. LEDs mounted on different boards: (b, top) FR4 boards (electrode layout Sch1 and Sch2) and (b, bottom) MCPCB/diamond boards (electrode layout Sch1).

Table 1
Structure, dimensions, and thermal conductivity (λ) of the different boards layers.

Board	Layer (top to bottom)	Material	Thickness μm	Thermal conductivity W/(m·K)
FR4 [25]	Metallization	Cu	70	400
	Dielectric	FR4	800/1600	0.81–1.059 (in-plane) [26,27] 0.29–0.343 (out-of-plane) [26,27]
MCPCB [25]	Metallization	Cu	70	400
	Dielectric	Unknown	100	2.2
	Metal core	Al	1588	150
Diamond [28]	Metallization	Ti/W/Au	1 (Au layer)	318 [29]
		Ag conductive ink	Unknown	Unknown
	Dielectric	Diamond	300	1800

the cylinder. In the case of square PCBs, $L = \sqrt{A_B}$, where A_B is the area of the board.

Additional cooling of the board due to thermal radiation can be estimated by using the Stefan-Boltzmann law:

$$P_{rad} = \epsilon_{eff} \cdot \sigma \cdot \left((T - T_{0K})^4 - (T_{amb} - T_{0K})^4 \right) \cdot A_B, \quad (2)$$

where P_{rad} is the radiative thermal transfer power, T and T_{amb} are the temperatures of the board and the ambient, respectively, $T_{0K} = -273.15^{\circ}$C, $\sigma \approx 5.67 \times 10^{-8}$W/(m$^2 \cdot$ K^4) is the Stefan-Boltzmann constant, and ϵ_{eff} is the effective emissivity factor of the board surface.

Besides the extra heat loss due to convection and radiation, there is another parasitic channel of heat dissipation, which exists in the experimental setup shown in Fig. 2: the wires that connect the LED to the current source. The influence of these wires on the temperature measurements is important for thicker boards with lower λ. To take into account this effect, one has to solve the problem of heat dissipation through a wire with certain thermal resistance per unit length and certain heat conductance to the ambient air (also per unit length of wire). To estimate this heat conductance for vertical wires, we can use Eq. (1), where $L = l_w$ is the wire length. We can assume that the far ends of the wires are at the ambient temperature. Then, for the heat power

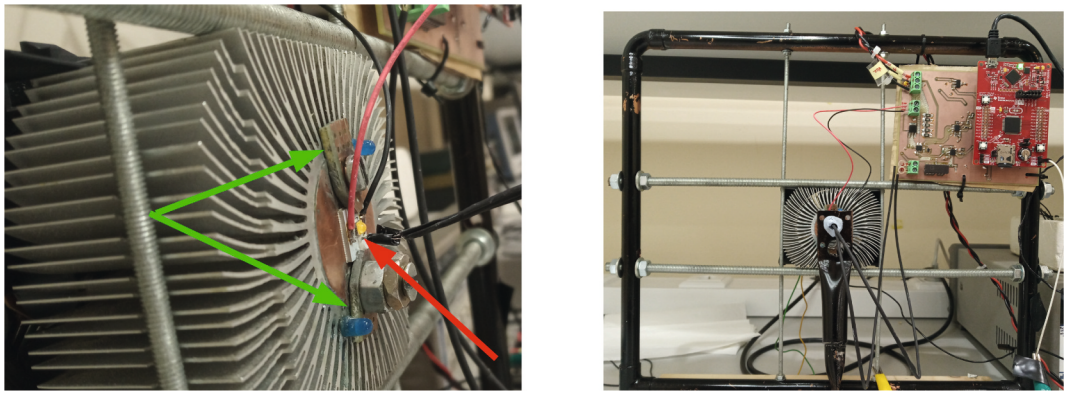

Fig. 2. (a) MCPCB on HS; FR4 flaps (green arrows) facilitate boards assembling/removal and a thermocouple (red arrow) touches the LED case. (b) HS assembled with metallic frame.

dissipated through the wires we can write (see Appendix A):

$$P_w = 2\cdot\pi\cdot\left(T - T_{amb}\right)\cdot\sqrt{2\lambda_w h_{c,av} r_w^3}\cdot coth\left(l_w\cdot\sqrt{\frac{2h_{c,av}}{\lambda_w r_w}}\right), \quad (3)$$

where λ_w is the λ of the wire material (Cu), r_w is the wire radius, and $h_{c,\,av}$ is the average value of the heat transfer coefficient along the wire. An average has to be taken because the temperature is varying along the wire. A good approximation to $h_{c,\,av}$ can be obtained from Eq. (1) with $\Delta T = (T - T_{amb})/2$. The coefficient 2 in front of Eq. (3) is due to the fact that there are two wires of the same length and diameter.

Taking into account the heat dissipation mechanisms considered above, we arrive at the equivalent heat conduction network shown in Fig. 3. In this network, R_{JC} is the equivalent thermal resistance between the p-n junction of the LED and its case, $R_{B,1}$ is the thermal resistance across the board, for the heat flux that is concentrated under the LED's case, R_M is the thermal resistance of the metal traces that connect the thermal pad under the LED to the large thermal pads at the edges of the board (if present), $R_{B,2}$ is the thermal resistance for the heat flux concentrated under the mentioned pads, R_{HS} is the thermal resistance of the HS, and R_{ex} is the (generally, temperature-dependent) resistance that describes the extra heat dissipation through convection, radiation, and feeding wires. In the board configurations without extra thermal pads, R_M and $R_{B,2}$ should be excluded from the network. The value of R_{JC} is given by the LED manufacturer, and the values of $R_{B,i}$, $i = 1, 2$ and R_M are found as follows:

$$R_{B,i} = \frac{h}{\lambda_B A_i}, \quad R_M = \frac{l_{tr}}{2w_{tr}t_{tr}\lambda_M}, \quad (4)$$

where λ_M and λ_B are the thermal conductivities of the metallization layer and the board dielectric, respectively, h is the board thickness, A_1 is the total area of the contact and thermal pads near and under the LED's base (including the pads for wire soldering), A_2 is the total area of the two exterior thermal pads (which is the same as twice the area of a single pad; the coefficient 2 in the denominator of R_M is for the same reason), and l_{tr}, w_{tr}, and t_{tr} are the length, width, and thickness of the metal traces, respectively.

In the equivalent circuit of Fig. 3, T_J is the junction temperature, T_{SP} is the temperature at the soldering point, T_{HS} is the temperature at the HS, and $T_0 = T_{amb}$ is the ambient temperature. P_{Th} is the heat generation power at the LED's junction.

To solve for the unknown temperatures in this circuit, we consider the following system of equations:

$$T_J - T_{SP} = R_{JC}\cdot P_{Th}, \quad (5)$$

$$T_{SP} - T_{HS} = (P_{Th} - P_{ex})\Big/\left(R_{B,1}^{-1} + \left(R_M + R_{B,2}\right)^{-1}\right), \quad (6)$$

$$T_{HS} - T_{amb} = R_{HS}\cdot(P_{Th} - P_{ex}), \quad (7)$$

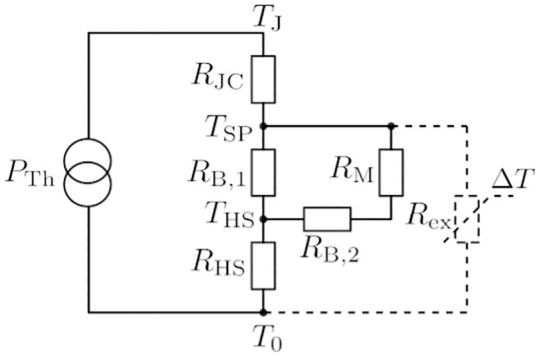

Fig. 3. The equivalent circuit of the heat transfer corresponding to the experimental setup from Fig. 2b.

$$P_{ex} = h_{c,B}\cdot(T_{SP} - T_{amb})\cdot A_B + P_{rad} + P_w, \quad (8)$$

where P_{ex} denotes the heat flux through R_{ex} and $h_{c,B}$ is the convection coefficient for the board, Eq. (1), with $\Delta T = T_{SP} - T_{amb}$ and $L = \sqrt{A_B}$. Analogously, when using the expressions for P_{rad} and P_w [Eqs. (2) and (3)], we assume that $T = T_{SP}$.

In this system, the first three equations are linear. The fourth equation is nonlinear in the temperature variables. To simplify the following considerations, without any loss of generality, we may assume that the HS resistance, R_{HS}, is negligibly small: $R_{HS} \approx 0$. Then, $T_{HS} \approx T_{amb}$. Then, from the second equation we obtain:

$$P_{ex} = P_{Th} - \left(R_{B,1}^{-1} + \left(R_M + R_{B,2}\right)^{-1}\right)\cdot(T_{SP} - T_{amb}). \quad (9)$$

By substituting Eq. (9) to Eq. (8) we obtain a nonlinear equation for T_{SP} that can be solved numerically.

4. Results and discussion

The evolution of T_{SP} as a response to a 700 mA current step is shown in Fig. 4a. The data for FR4/MCPCB and diamond boards were acquired during 300 and 1500 s, respectively; curves obtained at different current levels show a similar trend. The steady-state T_{SP} values for all the boards were obtained by fitting the experimental curves with a 2nd-order exponential (yellow curves). T_J was estimated using the expression:

$$T_J = T_{SP} + P_{Th}\cdot R_{JC}, \quad (10)$$

with P_{Th} the thermal power (calculated as 75 % of the electric power [1]) and R_{JC} the thermal resistance between junction and case (6.5 °C/W according to the data sheet). The values of T_{SP} and T_J obtained at 350 and 700 mA with the different boards are listed in Table 2. As expected, the highest T_J values were obtained for the thicker FR4 board without thermal pads (FR4_Sch1_1.6 mm): 76.0 (142.7) °C at 350 (700) mA. When the board thickness was reduced to 0.8 mm (FR4_Sch1_0.8 mm), T_J decreased to 65.1 (118.1) °C for the same current levels. The inclusion of thermal pads at the top surface of FR4 boards promoted the transfer of heat to the environment by convection/radiation and reduced T_J by 23.0/16.2 °C (thickness 1.6/0.8 mm) at 350 mA and 51.3/39.9 °C (thickness 1.6/0.8 mm) at 700 mA. The thermal pads were shown to have a larger impact on T_J than the board thickness; this is due to the different in-plane and out-of-plane λ values of FR4 boards. These results suggest that thermal pads should be included whenever possible; by taking advantage of the higher out-of-plane λ of the FR4, the thermal pads effectively promote the transfer of heat to the environment. When the LED was mounted on a MCPCB (as suggested by the manufacturer), T_J decreased to 41.8 (60.4) °C at 350 (700) mA. This reflects the significantly larger out-of-plane λ of the metal core in comparison to the FR4 layer (150 against 0.29–0.343 W/(m·K)). T_J further decreased 7.3 (13.0) °C for the same current levels when the MCPCB was replaced with a diamond board.

The results of the analytical model are presented in Table 2 alongside the corresponding experimental results. For LEDs mounted on 1.6 and 0.8 mm-thick FR4 boards, the results of the analytical model can be made consistent with the experimental results after adjusting the effective value of λ of the FR4 substrate. Although the variation of the ambient temperature during the measurements may influence the comparison of these results, in the analytical calculations we assumed a fixed ambient temperature (see Table 2). Under these assumptions, we obtain that for the thicker board the effective value is $\lambda_B = 0.5$ W/(m·K), and for the thinner one, $\lambda_B = 0.35$ W/(m·K). Higher effective λ value for the thicker board can be explained by a more pronounced lateral spreading of the heat flux inside the thicker board due to the high anisotropy of FR4 materials. The obtained effective values are within the typical range of λ of FR4 substrates [0.3 W/(m·K) for the out-of-plane and 0.9 W/(m·K) for the in-plane component [26,27]]. At high LED

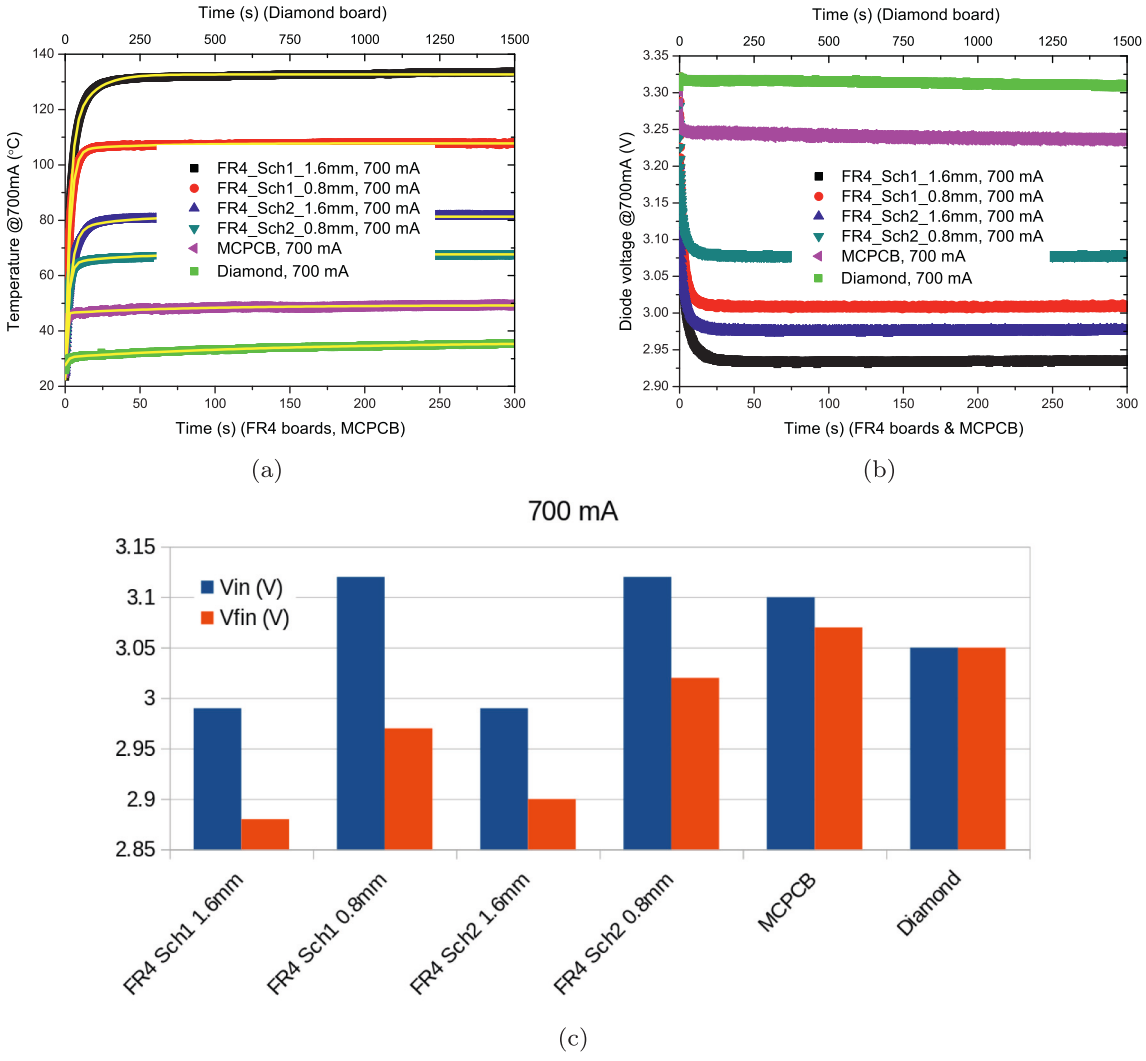

Fig. 4. (a) Evolution of T_{SP} as a response to 700 mA current steps. Yellow lines: curves obtained by fitting to a second-order exponential. (b) Evolution of diode voltage as a response to 700 mA current steps. (c) Initial and final values of LED voltage for 700 mA.

Table 2
Steady-state T_{SP} and T_J for the different boards and for different current levels.

	Board	Current (mA)			
		350		700	
		Exp.	Theor.	Exp.	Theor.
T_{SP} (°C)	FR4 Sch1 1.6 mm	71.1	70.0[a]	132.7	118[a]
	FR4 Sch1 0.8 mm	60.0	61.5[b]	107.8	102[b]
	FR4 Sch2 1.6 mm	48.1	49.9[a]	81.3	79.9[a]
	FR4 Sch2 0.8 mm	43.7	44.6[b]	67.7	69.2[b]
	MCPCB	36.5	35.2	49.3	51.5
	Diamond board	29.3	(See in text)	36.1	(See in text)
T_J (°C)	FR4 Sch1 1.6 mm	76.0	75.9[a]	142.7	128[a]
	FR4 Sch1 0.8 mm	65.1	66.6[b]	118.1	112[b]
	FR4 Sch2 1.6 mm	53.0	54.8[a]	91.4	90.0[a]
	FR4 Sch2 0.8 mm	48.9	49.7[b]	78.2	79.8[b]
	MCPCB	41.8	40.4	60.4	62.5
	Diamond board	34.5	(See in text)	47.4	(See in text)

[a] Assuming $\lambda_B = 0.5$ W/(m·K) and $T_{amb} = 20^{\circ}$C.
[b] Assuming $\lambda_B = 0.35$ W/(m·K) and $T_{amb} = 20^{\circ}$C.

currents, the difference between the experimentally obtained temperature values and the ones predicted by the analytical model is higher. This is expected, because the analytical model does not take into account the variation of LED's light emitting efficiency with temperature. The model also neglects the temperature dependence of λ of board materials.

We have found that in the case of the diamond board, the total thermal resistance between the LED's thermal pads and the ambient is dominated by the HS resistance. In this case, the complete equivalent model shown in Fig. 3 reduces to just a series connection of $R_{JC} = 6.5$ K/W, $R_{B,1} = 0.04$ K/W, and R_{HS}. From the temperature values measured at the beginning of the horizontal plateau in the diamond curves (see Fig. 4a), the HS resistance can be roughly estimated as $R_{HS} \gtrapprox 5$ K/W.

The evolution of the LED voltage as a response to a 700 mA current step is shown in Fig. 4c. For a given board, the LED voltage decreases as T_{SP} (and consequently T_J) increases. The maximum difference between the initial and final voltage values occurs with board FR4_Sch1_0.8 mm and not with the board that induces the highest steady-state T_J (FR4_Sch1_1.6 mm). In addition, when comparing the performance of the different boards, it can be seen that the steady-state value of the LED voltage does not decrease monotonically with the steady-state T_J, as could be initially expected. The *I–V* relationship in a p-n diode is given by the modified Shockley equation [31]:

$$I = I_S \cdot \left[exp\left(\frac{V - I \cdot R_S}{n \cdot V_T} \right) - 1 \right], \tag{11}$$

where I_S is the saturation current, V_T the thermal voltage, n the ideality factor, and R_S the series resistance. Here, n accounts for phenomena such

as generation and recombination of carriers in the depletion layer, high-injection condition that may occur even at relatively small forward bias, tunneling of carriers between states in the bandgap, and surface effects, whereas R_s reflects the parasitic resistances of contacts and cladding layers. For small current levels (when the effect of the internal series resistance in negligible), the temperature dependence of the voltage drop across a p-n junction is given by [32]:

$$\frac{dV}{dT} = \frac{V}{T} - \frac{q \cdot E_G + n \cdot l \cdot V_T}{T}, \tag{12}$$

where q is the electron charge, E_G the nominal bandgap, l the power factor in the temperature dependence of the square of the intrinsic carrier concentration n_i^2, and T the absolute junction temperature. However, the GaN-based LEDs studied in this paper are composed of a double heterojunction and multiple quantum wells. Besides the generation/recombination of the carriers (the dominant effect in p-n homojunctions), other charge transport processes may take place, such as thermionic emission [31], tunneling, surface states [33], Poole-Frenkel emission, hopping [34,35], and space-charge current limitation [36]. Each of these processes has its own temperature dependency, which prevents the derivation of an equation that expresses accurately the temperature-dependency of the diode voltage. In addition, the level of current that flows through the LED is significant and the voltage drop across the series resistance should not be neglected. At room temperature and 350 (700) mA this value is 0.13 (0.26) V (assuming $R_s = 0.365$ Ω [37]). Unlike what happens with Si, the temperature increase may cause a decrease in the resistivity of both p [38] and n-type [39] GaN layers due to a more complete activation at higher temperatures. This means that, as temperature increases, the voltage drop across R_s may decrease. Since the temperature dependence of the voltage drop across the junction itself and across R_s are different, the LED voltage may not show a monotonic dependency on T_J.

T_J has a tremendous impact on the lifetime of an LED. The mean time to failure (MTTF) is defined as the point at which the light output decreases to a given value, usually 70 % of the initial intensity [32]. The MTTF of a device can be calculated using the Black model [40,41] as:

$$MTTF = I_0 \cdot J^{-n} \cdot exp\left(\frac{q \cdot E_a}{k_B \cdot T}\right), \tag{13}$$

where I_0 is a constant, J the current density, n a scaling factor, q the electron charge, E_a the activation energy of the failure mechanisms (in eV), k_B the Boltzmann constant, and T the junction absolute temperature. Due to the unavailability of constants I_0 and n, the LED MTTF cannot be calculated directly. Instead, the decrease in the lifetime of an LED operating at higher temperature can be calculated by computing the acceleration factor (AF) as the ratio of the MTTFs under nominal operating conditions and at elevated operating temperatures. The AF can thus be defined as:

$$AF = \frac{TTF_{nom}}{TTF_{st}} = \left(\frac{J_{st}}{J_{nom}}\right)^n \cdot e^{\frac{q \cdot E_a}{k_B}\left(\frac{1}{T_{nom}} - \frac{1}{T_{st}}\right)} \tag{14}$$

where J_{nom} (T_{nom}) and J_{st} (T_{st}) are the current level densities (junction temperature) at nominal and stress conditions, respectively. In the current case, the AF allows the estimation of the lifetime increase/decrease when the MCPCB (the board suggested by the manufacturer) is replaced with other boards. For a given current level, the AF can be calculated as:

$$AF_{MCPCB} = \frac{TTF_{MCPCB}}{TTF_{board}} = e^{\frac{q \cdot E_a}{k_B}\left(\frac{1}{T_{J,MCPCB}} - \frac{1}{T_{J,board}}\right)}, \tag{15}$$

where $T_{J,\,MCPCB}$ and $T_{J,\,board}$ is the junction temperature with the MCPCB and with other boards, respectively.

The E_a of GaN failure mechanisms depends on the processes and materials used by the manufacturer [41]. In the lack of data relative to Cree LEDs, the AF was calculated for the minimum (1.05 eV) and maximum (2.5 eV) values of E_a found in the literature and for two levels of current, 350 and 700 mA. The results are presented in Fig. 5.

When the LED is mounted on an FR4 board, T_J for a given current increases in comparison with T_J with the MCPCB – and the lifetime consequently decreases. When operated at 350 mA and considering the lowest E_a (1.05 eV, which corresponds to the slowest aging), the LED ages twice as fast if mounted on the thinner board with thermal pads (FR4_Sch2_0.8 mm) and 44 times faster if mounted on the thicker board without thermal pads (FR4_Sch1_1.6 mm). At 700 mA the aging speed increases six and 1000 times for the same boards. For the highest E_a the LED ages eight (350 mA) and 80 (700 mA) times faster when mounted on board FR4_Sch2_0.8 mm. With the FR4_Sch1_1.6 mm board AF scales to a few thousand. If the use of an MCPCB is not an option, the LED should be mounted on the thinnest available FR4 board – and thermal pads should cover the entire area of the board without tracks. These results can be extrapolated to any power device.

On the other hand, the MTTF increases significantly when the LED is mounted on the diamond board (in comparison with the MCPCB). For the lowest E_a, MTTF increases 60 (80) % for a current of 350 (700) mA. For 2.5 eV, the AF is as low as 0.11 (0.03) (350 (700) mA). If mounted on the diamond board, the LED could be operated at 700 mA – and this would have a negligible impact in comparison to the MTTF of a similar LED mounted on a MCPCB and operated at 350 mA.

These results show that, for highly demanding applications in terms of power/lifetime, the use of diamond boards should be considered. However, some issues still remain unaddressed. One of them is the high cost of these boards in comparison with standard MCPCBs. Replacing MCPCBs in common luminaries with diamond boards, for instance, is not realistic. However, for high end applications – such as the case of the space industry – the use of diamond boards can bring an additional

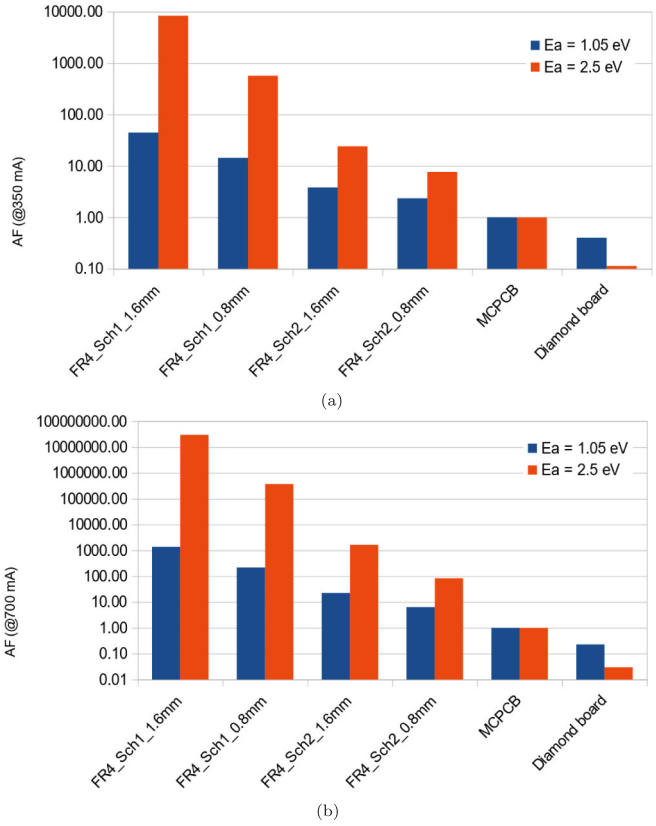

Fig. 5. Acceleration factor induced by replacing the MCPCB with each of the other boards for a current level of (a) 350 and (b) 700 mA.

advantage. An example is the development and commercialization of the GaN-on-diamond technology to fabricate HEMTs and power amplifiers, radio, and transmitter modules for space satellites by Qorvo and Akash Systems. However, in the GaN-on-diamond technology the diamond is integrated at the wafer level, whereas this paper focuses on using diamond at board level.

Another issue that was encountered during this work is the high electrical resistance of the electric pads. Diamond boards with specific electrical pads can be purchased from different manufacturers around the world simply by supplying a file with the required electrode layout. A thin layer of Ti/W guarantees the adhesion of the metal electrode to the diamond surface - and the final Au layer allows the integration with the device. However, this Au layer is much thinner than the Cu layer of a regular PCB. The track resistance of a 1 mm × 1 mm patch of Au is 22 mΩ, 100 times higher than that of a similar PCB patch. This Au layer is easily removed from the metal stack and, if this happens, an extremely thin (a few tenths of nm) Ti/W layer with a very high track resistance is all that is left to solder the components. In addition, the regular solders are prepared to be used on Cu surfaces, which may bring an additional difficulty during the soldering step.

Finally, diamond plates feature a very low coefficient of thermal expansion (CTE, $1 \times 10^{-6}/^{\circ}C$ at room temperature). On one side this is an advantage, since diamond boards show a greater dimensional stability than common FR4 boards (with CTE = $9.2 \times 10^{-6}/^{\circ}C$). Nevertheless, the CTE of the device carrier should also be considered; in case it is significantly higher, thermal cycling can lead to the early failure of the solder layer.

5. Conclusions

The junction temperature of Cree cold white XLamp XB-D LEDs mounted on 1 cm^2 FR4, MCPCB, and diamond boards was measured for different current ratings. The experimental results were additionally validated with an analytical thermal model. Compared with the MCPCBs commonly used to mount power LEDs, FR4 boards show a much poorer thermal performance, as expected; in the worst case, and taking as a reference the MCPCB board, the junction temperature increases ≃34 and ≃72 °C for 350 and 700 mA forward current, respectively. The replacement of the MCPCB with diamond decreases the junction temperature, for the same current levels, by ≃19 and ≃24 °C, respectively. The variation in the junction temperature has a tremendous impact on the lifetime of the LEDs. Depending on the activation energy of the aging processes, LEDs mounted on the diamond board will age 60–90 % slower for 350 mA forward current and 90–99 % slower for 700 mA, in comparison with those mounted on the MCPCB. There results show the potential of using diamond boards; however, their high cost in comparison with MCPCBs limits their use to specific and high demanding scenarios, such as space applications.

Declaration of competing interest

The authors declare that they have no known competing financial interests or personal relationships that could have appeared to influence the work reported in this paper.

Acknowledgment

This work is funded by FCT/MCTES through national funds and when applicable co-funded by EU funds under the projects UIDB/50008/2020-UIDP/50008/2020 and UID/EEA/50008/2019.

Appendix A. Heat dissipation through wires

The heat conduction equations for a vertical wire whose top end is kept at a fixed temperature T_{amb} and the bottom end at the temperature $\mathscr{T}(0) + T_{amb}$, $\mathscr{T}(0) \rangle 0$, can be written as follows (x is the coordinate along the wire):

$$\frac{d\mathscr{T}(x)}{dx} = -\frac{P(x)}{\lambda_w \pi r_w^2}, \tag{A.1}$$

$$\frac{dP(x)}{dx} = -2\pi r_w h_{c,av} \mathscr{T}(x). \tag{A.2}$$

The solution of this system of equations that satisfies the boundary conditions at the two ends of the wire is

$$\mathscr{T}(x) = \frac{\mathscr{T}(0) sinh(\alpha(l_w - x))}{sinh(\alpha l_w)}, \tag{A.3}$$

$$P(x) = \frac{P(0) cosh(\alpha(l_w - x))}{cosh(\alpha l_w)}, \tag{A.4}$$

where $\alpha = \sqrt{\frac{2h_{c,av}}{\lambda_w r_w}}$. Eq. (3) can be obtained by substituting Eqs. (A.3)–(A.4) into Eq. (A.1) with $P(0) = P_w/2$ and $\mathscr{T}(0) = T - T_{amb}$.

References

[1] Cree, Thermal management of cree XLamp application note, URL: https://www.cree.com/led-components/media/documents/XLampThermalManagement.pdf, 2015.

[2] D. Zhong, H. Qin, C. Wang, Z. Xiao, Thermal performance of heatsink and thermoelectric cooler packaging designs in LED, in: Proceedings – 2010 11th International Conference on Electronic Packaging Technology and High Density Packaging, ICEPT-HDP 2010 (100), 2010, pp. 1377–1381, https://doi.org/10.1109/ICEPT.2010.5582819.

[3] N. Wang, C. Gao, Q. Lu, H. Jia, G. Sui, X. Gao, in: Study on the Heat Disspation System Using Thermoelectric Cooling Based on Energy Harvesting for High-power LED, 2019 Cross Strait Quad-Regional Radio Science and Wireless Technology Conference, CSQRWC 2019 – Proceedings, 2019, pp. 1–2, https://doi.org/10.1109/CSQRWC.2019.8799348.

[4] P. Liu, Y. Li, X. Jian, C. Jing, M. Li, S. Ding, G. Zhang, Thermal simulations of a UV LED module with nanosilver sintered die attach process on graphene-coated copper substrates, in: 2019 16th China International Forum on Solid State Lighting and 2019 International Forum on Wide Bandgap Semiconductors China, SSLChina: IFWS 2019, 2019, pp. 93–97, https://doi.org/10.1109/SSLChinaIFWS49075.2019.9019813.

[5] B. Paul, M. Mathew, P.G. Shripad, Modelling and thermal analysis of honey comb heat sink for LEDs in street lighting applications, in: Proceedings of the International Conference on Inventive Systems and Control, ICISC 2017, 2017, pp. 1–5, https://doi.org/10.1109/ICISC.2017.8068618.

[6] Y. Luo, B. Yu, C. Zhou, X. Wang, Micro heatpipe integrated with LED silicon substrate, in: 16th International Conference on Electronic Packaging Technology, ICEPT 2015, 2015, pp. 85–88, https://doi.org/10.1109/ICEPT.2015.7236550.

[7] L. Xu, R. Liang, J. Dai, H. Long, S. Wang, J. Chen, J. Xu, X. Li, C. Chen, Reduction of structural thermal resistance for deep ultraviolet light-emitting diodes fabricated on AlN ceramic substrate via copper- filled thermal holes, IEEE Trans. Compon. Packag. Manuf. Technol. 8 (12) (2018) 2107–2112, https://doi.org/10.1109/TCPMT.2018.2812226.

[8] E. Juntunen, O. Tapaninen, A. Sitomaniemi, M. Jamsa, V. Heikkinen, M. Karppinen, P. Karioja, Copper-core MCPCB with thermal vias for high-power COB LED modules, IEEE Trans. Power Electron. 29 (3) (2014) 1410–1417, https://doi.org/10.1109/TPEL.2013.2260769.

[9] D. Pounds, R.W. Bonner, High heat flux heat pipes embedded in metal core printed circuit boards for LED thermal management, in: Thermomechanical Phenomena in Electronic Systems -Proceedings of the Intersociety Conference, 2014, pp. 267–271, https://doi.org/10.1109/ITHERM.2014.6892291.

[10] L. Huang, Y.C. Shih, F.G. Shi, Effectiveness of polymer composite-induced passive radiation cooling in thermal management of LED emitters and modules: impact on hotspot elimination, IEEE Trans. Compon. Packag. Manuf. Technol. 7 (9) (2017) 1453–1458, https://doi.org/10.1109/TCPMT.2017.2703826.

[11] R.H. Horng, C.C. Chiang, Y.L. Tsai, C.P. Lin, K. Kan, H.I. Lin, D.S. Wuu, Thermal management design from Chip to package for high power InGaN/Sapphire LED applications, Electrochem. Solid-State Lett. 12 (6) (2009), H222, https://doi.org/10.1149/1.3110040.

[12] R. Liang, J. Zhang, S. Wang, Q. Chen, L. Xu, J. Dai, C. Chen, Investigation on thermal characterization of eutectic flip-chip UV-LEDs with different bonding voidage, IEEE Trans. Electron Devices 64 (3) (2017) 1174–1179, https://doi.org/10.1109/TED.2017.2656240.

[13] M.Y. Tsai, C.Y. Tang, C.Y. Yen, L.B. Chang, Bump and underfill effects on thermal behaviors of flip-chip LED packages: measurement and modeling, IEEE Trans. Device Mater. Reliab. 14 (1) (2014) 161–168, https://doi.org/10.1109/TDMR.2013.2248365.

[14] M. Shatalov, A. Chitnis, P. Yadav, M.F. Hasan, J. Khan, V. Adivarahan, H. P. Maruska, W.H. Sun, M.A. Khan, Thermal analysis of flip-chip packaged 280 nm nitride-based deep ultraviolet lightemitting diodes, URL: Appl. Phys. Lett. 86 (20) (2005) 201109, https://doi.org/10.1063/1.1927695.

[15] C.Y. Tang, M.Y. Tsai, C.C. Lin, L.B. Chang, Thermal measurements and analysis of flip-chip led packages with and without underfills, in: International Microsystems Packaging Assembly and Circuits Technology Conference, IMPACT 2010 and International 3D IC Conference, Proceedings (May 2018), 2010, pp. 2–6, doi: 10.1109/IMPACT.2010.5699638.

[16] S. Kyatam, L.N. Alves, S. Maslovski, J.C. Mendes, Impact of die carrier on reliability of power LEDs, IEEE J. Electron Devices Soc. 9 (September) (2021) 854–863, https://doi.org/10.1109/JEDS.2021.3115027.

[17] K.L. Chun, M.J. Dai, C.K. Yu, S.L. Kuo, High efficiency siliconbased high power LED package integrated with micro- thermoelectric device, in: Proceedings of Technical Papers - 2007 International Microsystems, Packaging, Assembly and Circuits Technology Conference, IMPACT (c), 2007, pp. 29–33, https://doi.org/10.1109/IMPACT.2007.4433562.

[18] B. Fan, H. Wu, Y. Zhao, Y. Xian, B. Zhang, G. Wang, Thermal study of high-power nitride-based Flip-chip light-emitting diodes, IEEE Trans. Electron Devices 55 (12) (2008) 3375–3382.

[19] J.J. Gracio, Q.H. Fan, J.C. Madaleno, Diamond growth by chemical vapour deposition, J. Phys. D. Appl. Phys. 43 (37) (2010), 374017, https://doi.org/10.1088/0022-3727/43/37/374017, 1–22.

[20] C.B. Swan, Improved performance of silicon avalanche oscillators mounted on diamond heat sinks, Proc. IEEE 55 (9) (1967) 1617–1618, https://doi.org/10.1109/PROC.1967.5915.

[21] P.H. Chen, C.L. Lin, Y.K. Liu, T.Y. Chung, C.Y. Liu, Diamond heat spreader layer for high-power thin-GaN light-emitting diodes, IEEE Photon. Technol. Lett. 20 (10) (2008) 845–847, https://doi.org/10.1109/LPT.2008.921826.

[22] Y. Fan, H. Guo, J. Xu, K. Chu, X. Zhu, C. Jia, F. Yin, X. Zhang, Pressure infiltrated Cu/diamond composites for LED applications, Rare Metals 30 (2) (2011) 206–210, https://doi.org/10.1007/s12598-011-0225-5.

[23] R. Xie, Z. Li, S. Guo, Z. Wang, H. Xue, High bandwidth GaN-based blue LEDs using ag-grating and diamond heat sink, Photonics Nanostruct. Fundam. Appl. 42 (2020), 100856, https://doi.org/10.1016/j.photonics.2020.100856. URL: doi: 10.1016/j.photonics.2020.100856.

[24] Cree, Cree XLamp XB-D LEDs datasheet. https://www.cree.com/led-components/media/documents/ds-XBD.pdf, 2015, 1–22.

[25] CREE, Optimizing PCB thermal performance for Cree XLamp XP LEDs, URL: https://www.cree.com/led-components/media/documents/XLamp_PCB_Thermal.pdf, 2014.

[26] K. Azar, J.E. Graebner, Experimental determination of thermal conductivity of printed wiring boards, in: Proceedings of the Twelfth IEEE SEMI-THERM Symposium, 1996, pp. 169–182, https://doi.org/10.1109/STHERM.1996.545107.

[27] F. Sarvar, N.J. Poole, P.A. Witting, I. Technology, M. Glamorgan, U. Kingdom, PCB glass-fibre laminates: thermal conductivity, J. Electron. Mater. 19 (12) (1990) 1345–1350.

[28] Diamond materials, the CVD diamond booklet, URL: http://www.diamond-materials.com/downloads/cvd_diamond_booklet.pdf, 2014.

[29] Engineers Edge, Thermal properties of metals, conductivity, thermal expansion, specific heat, URL: https://www.engineersedge.com/properties_of_metals.htm.

[30] Cengel Yunus, Ghajar Afshin, Cooling of electronic equipment, in: Y. Cengel, Afshin Ghajar (Eds.), Heat and Mass Transfer: Fundamentals and Applications, McGraw Hill Education, USA, 2015, pp. 15.1 – 15.69.

[31] S. Sze, K.K. Ng, Physics of Semiconductor Devices, 3rd Edition, Wiley-Interscience, 2007.

[32] J. Li, J. Wang, Z. Liu, A. Poppe, Solid state physics fundamentals of LED thermal behavior, in: C.J.M. Lasance, A. Poppe (Eds.), Thermal Management for LED Applications, Springer, 2014, pp. 15–52, https://doi.org/10.1007/978-1-4614-5091-7_2. Ch. Chapter 2.

[33] E.M. Bourim, J.I. Han, Electrical characterization and thermal admittance spectroscopy analysis of InGaN/GaN MQW blue LED structure, Electron. Mater. Lett. 11 (6) (2015) 982–992, https://doi.org/10.1007/s13391-015-5180-0.

[34] H. Morkoç, Handbook of nitride semiconductors and devices, in: Electronic and Optical Processes in Nitrides, Vol. 2, Wiley-VCH, Weinheim, 2008.

[35] Q. Shan, D.S. Meyaard, Q. Dai, J. Cho, E.Fred Schubert, J.Kon Son, C. Sone, Transport-mechanism analysis of the reverse leakage current in GaInN light-emitting diodes, Appl. Phys. Lett. 99 (25) (2011), 253506, https://doi.org/10.1063/1.3668104, 1–3.

[36] I. Prudaev, Y.L. Zubrilkina, Baktybaev, I.S. Romanov, Hopping transport of charge carriers in LEDs based on multiple InGaN/GaN quantum wells, Russ. Phys. J. 57 (9) (2015) 1246–1250, https://doi.org/10.1007/s11182-015-0370-7.

[37] Cree, Cree XLamp-XBD spice model, URL: https://cree-led.com/media/documents/XLamp-XBD-Spice.txt, 2021.

[38] Y. Xi, E.F. Schubert, Junction–temperature measurement in GaN ultraviolet light-emitting diodes using diode forward voltage method, Appl. Phys. Lett. 85 (12) (2004) 2163, https://doi.org/10.1063/1.1795351.

[39] J.R. Fernandez, C.Moysés Araújo, A.Ferreira Da Silva, J.R. Leite, B.E. Sernelius, A. Tabata, E. Abramof, V.A. Chitta, C. Persson, R. Ahuja, I. Pepe, D.J. As, T. Frey, D. Schikora, K. Lischka, Electrical resistivity and band-gap shift of Si-doped GaN and metal-nonmetal transition in cubic GaN, InN and AlN systems, J. Cryst. Growth 231 (3) (2001) 420–427, https://doi.org/10.1016/S0022-0248(01)01473-7.

[40] J.R. Black, Electromigration—a brief survey and some recent results, IEEE Trans. Electron Devices 16 (4) (1969) 338–347, https://doi.org/10.1109/T-ED.1969.16754.

[41] S.R. Bahl, A comprehensive methodology to qualify the reliability of GaN products, URL:, in: Application Note, 2015, pp. 1–9 http://www.ti.com/lit/wp/slyy070/slyy070.pdf.